

00005

CR 85006

INVESTIGATION OF THE POTENTIALITIES OF
PHOTOCHEMICAL LASER SYSTEMS

PART 2 - PRELIMINARY EXPERIMENTAL STUDIES

FINAL REPORT
CONTRACT NO. NAS 12-94

1 February 1966 through 31 January 1967

by

C. R. Giuliano, L. D. Hess, and J. D. Margerum

Hughes Research Laboratories
Malibu, California

prepared for

National Aeronautics and Space Administration
Electronic Research Center
Cambridge, Massachusetts

FACILITY FORM 602	N67-35020	
	(ACCESSION NUMBER)	(THRU)
	104722-25	1
	(PAGES)	(CODE)
CR-85006	76	
(NASA CR OR TMX OR AD NUMBER)	(CATEGORY)	

INVESTIGATION OF THE POTENTIALITIES OF
PHOTOCHEMICAL LASER SYSTEMS

PART 2 - PRELIMINARY EXPERIMENTAL STUDIES

by

C. R. Giuliano, L. D. Hess, and J. D. Margerum

TABLE OF CONTENTS

PART I — SURVEY AND ANALYSIS

	LIST OF ILLUSTRATIONS	ix
	LIST OF TABLES	xv
	ABSTRACT	xvi
I.	INTRODUCTION AND SUMMARY	1
II.	EXCITATION MECHANISMS	5
	A. Electronically Excited Photodissociative Species	5
	B. Vibrationally Excited Photodissociative Species	6
	C. Laser Gain Equations	8
	D. Association Processes Stabilized by Stimulated Emission	14
	E. Franck-Condon Pumping — Nonequilibrium Distribution of Molecular Vibrational States	20
	F. Combinations of Solar and Chemical Pumping	26
III.	SPECTROSCOPY	31
	A. Absorption Spectra and Potential Energy Diagrams	31
	B. Halogens	35
	C. Interhalogens	38
	D. Alkyl Halides	48
	E. Nitrosyl Halides	52
	F. Alkyl Nitroso Compounds	55
	G. Nitrogen Oxides	55
	H. Chlorine Oxides	58

I.	Cyanides	62
J.	Metal Carbonyls	67
K.	Sulfur, Selenium, and Tellurium Compounds	71
L.	Other Compounds	73
IV.	PHOTOCHEMISTRY	79
A.	Introduction	79
B.	Rate of Termolecular Atomic Recombinations	79
C.	Alkyl Halides: Iodine Atom Laser	88
D.	Deactivation of Excited Iodine Atoms	89
E.	Indirect Formation of Excited Iodine Atoms	97
F.	Iodine Monochloride	98
G.	Nitrosyl Chloride: Nitric Oxide Laser	99
H.	Nitrogen Dioxide	105
I.	Cyanogen: Cyanyl Radical Laser	107
J.	Carbon Monoxide Laser Systems	108
K.	Solar and Chemical Excitation of Carbon Dioxide	109
V.	EVALUATION OF SOLAR PUMPING	115
A.	Solar Excitation Rates for Photodissociative Systems	115
B.	Evaluation of Sun-Pumped Photodissociative Systems	119
C.	Sun-Pumped Solid State Lasers	129
VI.	SUMMARY OF PRELIMINARY EXPERIMENTAL STUDIES	131
VII.	CONCLUSIONS AND RECOMMENDATIONS	133
VIII.	REFERENCES	137

TABLE OF CONTENTS

PART 2 - PRELIMINARY EXPERIMENTAL STUDIES

	LIST OF ILLUSTRATIONS	ix
	LIST OF TABLES	xv
	ABSTRACT	xvi
IX.	EXPERIMENTAL PROGRAM	145
	A. Objectives	145
	B. Apparatus	145
	C. Photolysis of CF_3I : Iodine Atom Laser	154
	D. Photolysis of $NOCl$: Nitric Oxide Laser	166
	E. Photolysis of Other Compounds	176

LIST OF ILLUSTRATIONS
PART 1 — SURVEY AND ANALYSIS

Fig. 1.	Potential energy diagram for a photodissociative vibrational laser system	19
Fig. 2.	The transitions between potential energy curves for an electronically excited and ground-state diatomic molecule	21
Fig. 3.	Energy level diagram for an absorption band system with convergence and continuum	32
Fig. 4.	The transitions between potential energy curves for an electronically excited and ground-state diatomic molecule	32
Fig. 5.	Potential energy curves for the S_2 molecule	34
Fig. 6.	Absorption spectra of the halogens	36
Fig. 7.	Potential energy diagram for several states of the $I_2(g)$ molecule	37
Fig. 8.	Potential energy diagram of the lowest excited states in the Br_2 molecule	39
Fig. 9.	Absorption spectrum of IBr in the vapor phase at $25^\circ C$	40
Fig. 10.	Absorption spectrum of ICl in the vapor phase at $25^\circ C$	41
Fig. 11.	Absorption spectrum of $BrCl$ in the vapor phase at $25^\circ C$	42
Fig. 12.	Potential energy curves for the $^1\pi$ (normal) and $^3\pi$ states of ICl	44
Fig. 13.	Potential energy curves for the $^3\pi$ states showing how the $^3\pi_0^+$ state may predissociate above the level $v = 3$	46
Fig. 14.	Approximate potential energy curves of IBr	47
Fig. 15.	Absorption spectra of alkyl halides	49
Fig. 16.	The observed extinction coefficient curve of methyl iodide and the proposed resolution into two bands	50

Fig. 17.	The potential energy curves of the C-I link and the eigenfunction curves of some of the energy levels	51
Fig. 18.	Absorption spectrum of NOCl vapor at room temperature showing the 11 bands	53
Fig. 19.	Potential energy diagram of the NOCl molecule as a function of (NO)-Cl distance	54
Fig. 20.	Absorption spectra of CF_3NO and $(\text{CH}_3)_3\text{CNO}$	56
Fig. 21.	Absorption spectra ($1/\rho \log_{10} I_0/I$) of NO_2 and N_2O_4 versus wavelength and wave number, measured at 25°C	57
Fig. 22.	The extinction coefficients of dinitrogen trioxide at different liquid compositions, at 10°C	59
Fig. 23.	Approximate potential energy diagram for some probable electronic states of NO_2	59
Fig. 24.	Orbital energies in NO_2 relative to a nitrogen p orbital	60
Fig. 25.	Absorption spectrum of Cl_2O	60
Fig. 26.	Absorption spectra of chlorine oxides dissolved in carbon tetrachloride	61
Fig. 27.	Approximate potential energy curves showing the potential energy of the ICN molecule as a function of the carbon-iodine separation, for three electronic states	63
Fig. 28.	The potential energy diagram of CN	64
Fig. 29.	Absorption spectrum of $\text{CO}(\text{CN})_2$ vapor	64
Fig. 30.	Schematic representation of potential curves $V = F(\theta)$ for the A_2 and dissociative state of $\text{CO}(\text{CN})_2$	65
Fig. 31.	The energy level diagram and the term-level diagram of formaldehyde	66
Fig. 32.	Normal vibrations of an XYZ_2 molecule and their behavior for a reflection at the plane of symmetry through XY perpendicular to the plane of the molecule	68

Fig. 33.	The visible and ultraviolet spectrum of $\text{Fe}(\text{CO})_5$	69
Fig. 34.	Absorption spectrum of gaseous $\text{V}(\text{CO})_6$	70
Fig. 35.	The ultraviolet spectrum of gaseous $\text{Cr}(\text{CO})_6$	70
Fig. 36.	Values of extinction coefficient and of $\log a$ as a function of wavelength for $\text{Ni}(\text{CO})_4$	72
Fig. 37.	Absorption spectra of various sulfur chlorides	72
Fig. 38.	Ultraviolet absorption spectrum of S_2Cl_2	74
Fig. 39.	Ultraviolet absorption spectra of CSe_2 , CS_2 , and COS	74
Fig. 40.	The absorption spectrum of H_2S , H_2Se , and H_2Te	74
Fig. 41.	Absorption spectrum of O_3	75
Fig. 42.	Absorption spectrum for biacetyl [$\text{CH}_3\text{COCOCH}_3(\text{g})$], 25°C	77
Fig. 43.	Absorption spectrum of HI	77
Fig. 44.	Potential energy curves for the lowest electronic states of HI	78
Fig. 45.	Laser tube and cavity used by DeMaria and Ultee	90
Fig. 46.	Potential energy diagram for nitric oxide	100
Fig. 47.	Third order plot of photolysis back reaction $2\text{NO}(\text{g}) + \text{Cl}_2 \xrightarrow{k} 2\text{NOCl}(\text{g})$	104
Fig. 48.	Energy level diagram showing pertinent levels in CO_2 and N_2	110
Fig. 49.	(a) Solar emission spectrum. (b) Absorption spectrum of iodine monochloride. (c) Solar pumping rate constant of ICl	117
Fig. 50.	Schematic diagram for photodissociative laser system	121

LIST OF ILLUSTRATIONS

PART 2 - PRELIMINARY EXPERIMENTAL STUDIES

Fig. 51.	Photochemical laser apparatus	146
Fig. 52.	Flash photolysis photochemical laser apparatus	147
Fig. 53.	Vacuum system and gas handling apparatus	150
Fig. 54.	Schematic of gas handling system	151
Fig. 55.	CF ₃ I laser output (1.3 μ) at different pressures	155
Fig. 56.	CF ₃ I laser output (1.3 μ) at lower pressures	156
Fig. 57.	CF ₃ I laser output at different flashlamp discharge voltages	157
Fig. 58.	CF ₃ I laser output	159
Fig. 59.	CF ₃ I laser output at different excitation energies	159
Fig. 60.	CF ₃ I laser output with extreme cavity loss	160
Fig. 61.	CF ₃ I laser output with calibrated optical loss introduced in cavity	162
Fig. 62.	CF ₃ I laser output with calibrated optical loss in cavity at different excitation intensities	163
Fig. 63.	CF ₃ I laser output with calibrated optical loss in cavity	164
Fig. 64.	Variation of onset, termination, and duration of laser oscillation from CF ₃ I versus cavity loss	165
Fig. 65.	CF ₃ I gain in lower pressure region	167
Fig. 66.	CF ₃ I laser gain versus flashlamp intensity	168
Fig. 67.	Output from nitrosyl chloride photodissociative laser	169

Fig. 68.	Effect of excitation energy on NOCl laser output	171
Fig. 69.	Effect of excitation intensity on NOCl laser output	172
Fig. 70.	Laser output from nitrosyl chloride	173

LIST OF TABLES

PART 1 - SURVEY AND ANALYSIS

Table I.	Molecular Vibrational Transitions for Laser Action by Thermal Pumping Techniques	29
Table II.	The Reaction Paths of an Electronically Excited Simple Molecule	80
Table III.	The Rate Coefficient $k_1 \times 10^{-16}$ ($\text{cm}^6\text{-mole}^{-2}\text{-sec}^{-1}$) for Iodine Atom Recombinations at 20°C	84
Table IV.	The Rate Coefficient $k_1 \times 10^{-15}$ ($\text{cm}^6\text{-mole}^{-2}\text{-sec}^{-1}$) for Iodine Atom Recombination at High Temperatures	85
Table V.	The Rate Coefficient $k_1 \times 10^{-15}$ ($\text{cm}^6\text{-mole}^{-2}\text{-sec}^{-1}$) for Bromine Atom Recombination in Argon	85
Table VI.	Comparison of Calculated with Observed Recombination Rate Coefficients $k_r \times 10^{-15}$ ($\text{cm}^6\text{-mole}^{-2}\text{-sec}^{-1}$) at 300°K	87
Table VII.	Probability P of $\text{I}(^2\text{P}_{1/2})$ Deactivation by Collision	95
Table VIII.	Solar Pumping Rates	118
Table IX.	Evaluation of Sun-Pumped Photodissociative Systems	127

PART 2 - PRELIMINARY EXPERIMENTAL STUDIES

Table X.	Detectors Available for Photochemical Laser Studies	152
Table XI.	Broad-Band Infrared Filters	153

ABSTRACT

Photodissociative laser systems are proposed and evaluated with regard to their potential for conversion of solar radiation to monochromatic coherent emission. Spectroscopic and photochemical properties of several molecules which absorb light in the visible and near ultraviolet regions are reported, discussed, and compared with requirements for obtaining laser action. Additional mechanisms for achieving population inversions in these systems indirectly, such as Franck-Condon pumping and association processes stabilized by stimulated emission, are also discussed. Preliminary experimental studies are reported for methyl iodide and bromide, iodo- and bromocyanogen, iodine bromide, and nitrogen dioxide. Laser action was observed under a variety of experimental conditions from CF_3I and NOCl , but could not be detected in the initial studies conducted with other compounds. Chemical reversibility was demonstrated for the nitrosyl chloride system using mixtures of molecular chlorine and nitrosyl chloride.

SECTION IX

EXPERIMENTAL PROGRAM

A thorough discussion and analysis of the photochemical, kinetic, and laser behavior known about the molecules studied here is given in Part 1 of this report, which includes detailed literature references.

A. OBJECTIVES

The experimental part of this program is designed to complement and extend the information available for the analysis of solar pumped photochemical laser systems. The apparatus is set up for studies designed to observe laser emission from flash photolysis of gases under various conditions. The factors which are readily controlled are the pressure of the species being photolyzed, the pressure of other added gases such as helium, the intensity and total energy of the flash pulse, and the losses introduced into the cavity. Thus some measure can be made of the laser threshold as a function of pressure and pumping intensity, and the gain of the laser system can be estimated. The lifetime of the laser pulses is also measured, and the wavelength range can be estimated. Knowledge of the wavelength and the lifetime characteristics of emission is required to confirm the identity of the emitting species, so that the behavior under varying conditions can be predicted. Measurements of the pumping thresholds for laser action are particularly important with regard to the feasibility of achieving direct solar pumped photochemical lasers.

B. APPARATUS

1. Flash Photolysis System

A flash photolysis, photochemical laser apparatus has been designed and built for these studies. A drawing of the flash lamp and optical bench is shown in Fig. 51 and a photograph is shown in Fig. 52. The light source is a xenon filled quartz flash lamp

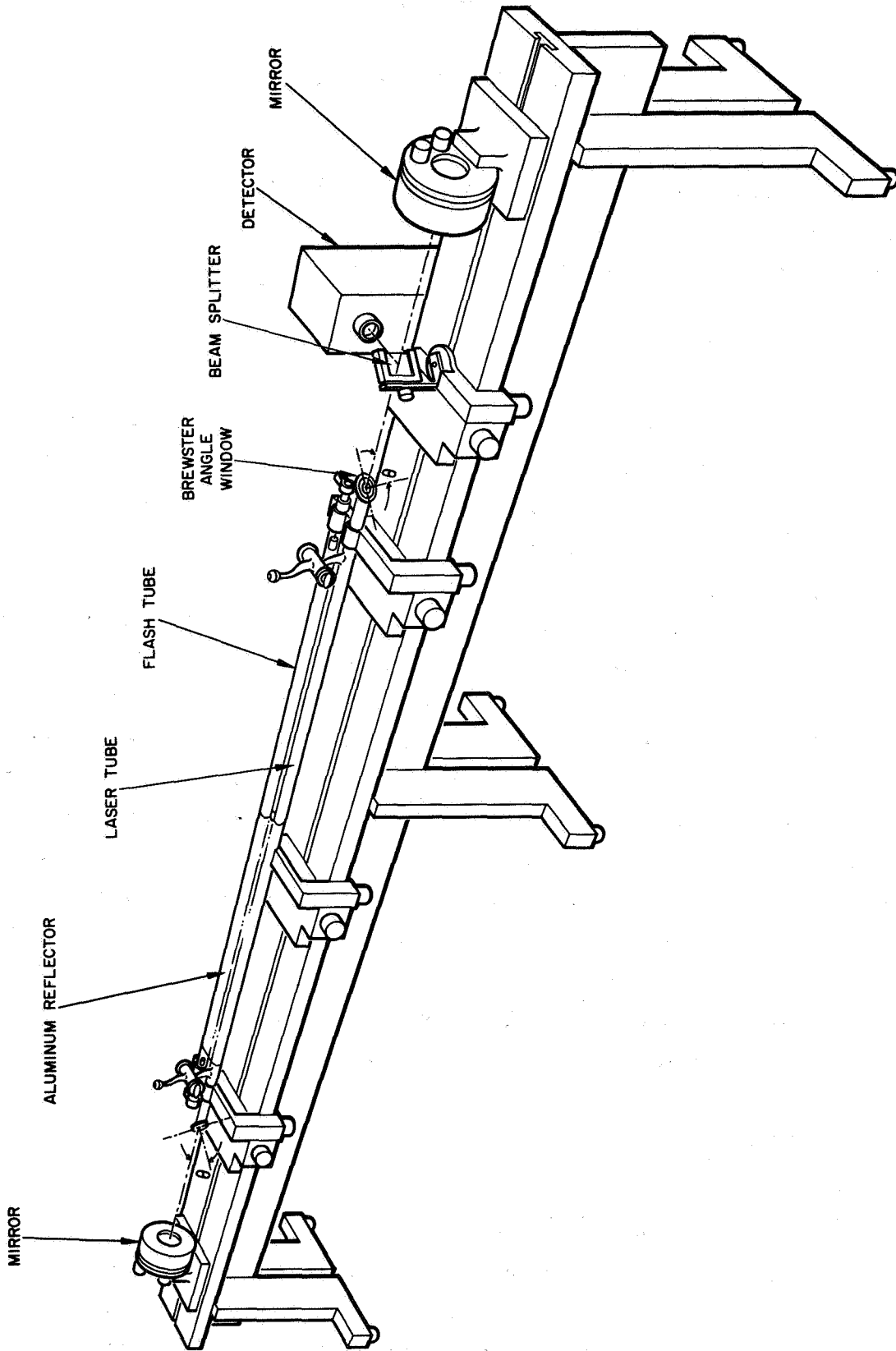


Fig. 51. Photochemical laser apparatus.

M 4966

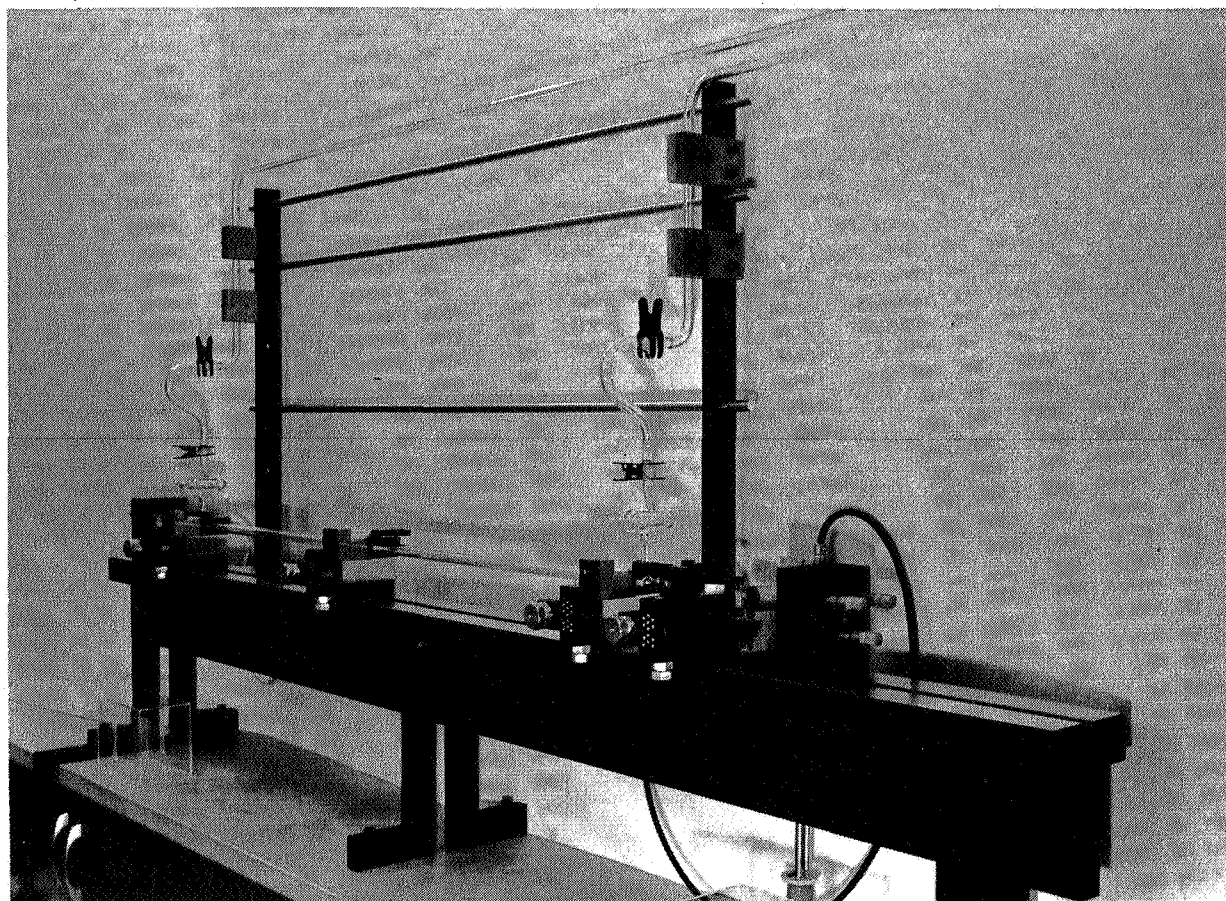


Fig. 52. Flash photolysis photochemical laser apparatus.

(PEK No. XE-16-2985) with a 1-m spacing between electrodes. It was designed for operation with a 3 msec pulse of 7000 J input energy (250 μ F at 7.5 kV) from a laser power supply (Hughes Model 350). This power supply delivers a square shaped pulse of 3 msec duration for its maximum output of 8000 J, although lower energy pulses can be delivered with shorter pulse lengths. However, it was found necessary to modify this power supply in order to obtain higher power flash intensities. The pulse-shaping inductances were removed from the circuit and the capacitors were allowed to discharge the flash tube with a typical exponential decay characteristic. Typically, 800 J are discharged (25 μ F at 8 kV) with a bandwidth of \sim 100 μ sec (FWHH). An alternate flash tube and power supply are being built to permit an additional increase in the power output of the flash discharge. This apparatus will use an 8 μ F capacitor discharged at 10 to 20 kV.

2. Optical Components

The flash lamp is coupled to a pyrex or quartz laser tube in a parallel configuration, with an aluminum foil reflector wrapped around the two tubes. The laser tube has a total length of 1.13 m and is situated in a semiconfocal optical cavity formed by gold coated mirrors spaced 1.6 m apart. One mirror is flat and the other is spherical with a 4 m radius of curvature. Sodium chloride windows are attached to the ends of the laser tube cut at a Brewster angle (56° for NaCl). The windows are sealed to the tube with Dow Corning Silastic 140 silicone adhesive, applied in a manner that reduces to a minimum the contact between the adhesive and the laser tube contents. No difficulty has been encountered in handling highly corrosive materials (NOCl, IBr, NO₂). A beam splitter of the same material as the laser tube windows and situated at a similar angle is used to divert a portion of the cavity radiation to the analyzing and detection apparatus. A Hughes Model 35 helium-neon

laser is attached to the optical bench using mounting apparatus with precision adjustments for alignment of the laser tube, mirrors, beam splitter, monochromator, and detectors.

3. Detectors, Optical Filters and Monochromators

Sensitive detection of pulsed infrared radiation becomes an increasingly difficult problem with increased wavelength of the radiation to be detected. Table X shows a list of detectors that are available for our studies. High detectivity and fast response are available in the near infrared. The PbS, InAs, and InSb detectors have been used initially, since their useful range coincides with the wavelength region expected for atomic iodine and bromine, and nitrosyl halides and nitric oxide emission. While InSb is a convenient detector at wavelengths up to 7.5 μ , gold doped germanium at low temperature is more sensitive and has a much faster response.

Analysis of the laser emission wavelength is also less convenient at longer wavelengths in the infrared. Two Bausch and Lomb low resolution monochromators with wavelength ranges of 0.7 to 1.6 μ and 1.4 to 3.2 μ will be used for the near infrared region. Initially, broadband infrared filters are used in conjunction with various detectors to isolate different spectral regions at longer wavelengths, as shown in Table XI. Later, an infrared spectrometer can be used to further identify the wavelength position of observed laser output.

4. Vacuum System, Gas Handling Equipment

The gas handling and vacuum equipment is shown in its assembly rack in Fig. 53 and is represented schematically in Fig. 54. This system is designed so that corrosive and toxic compounds such as NOCl and IBr can be handled conveniently. Mercury is excluded from the vacuum system, and nonreactive fluorocarbon stopcock grease (Ascolube F) is used throughout. Since the vapor pressure of this grease (10^{-5} Torr) is not very low, vacuum diffusion pumps were not used in our preliminary

M 5177

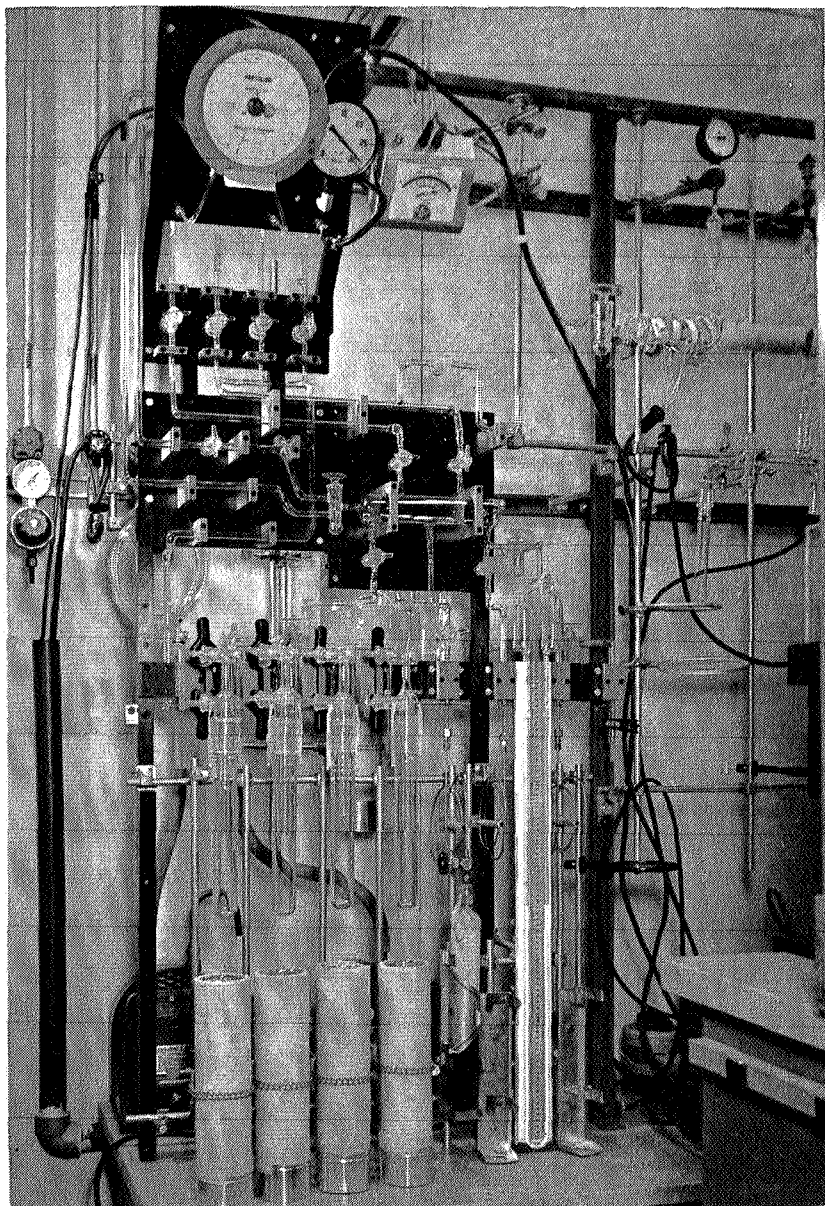


Fig. 53. Vacuum system and gas handling apparatus.

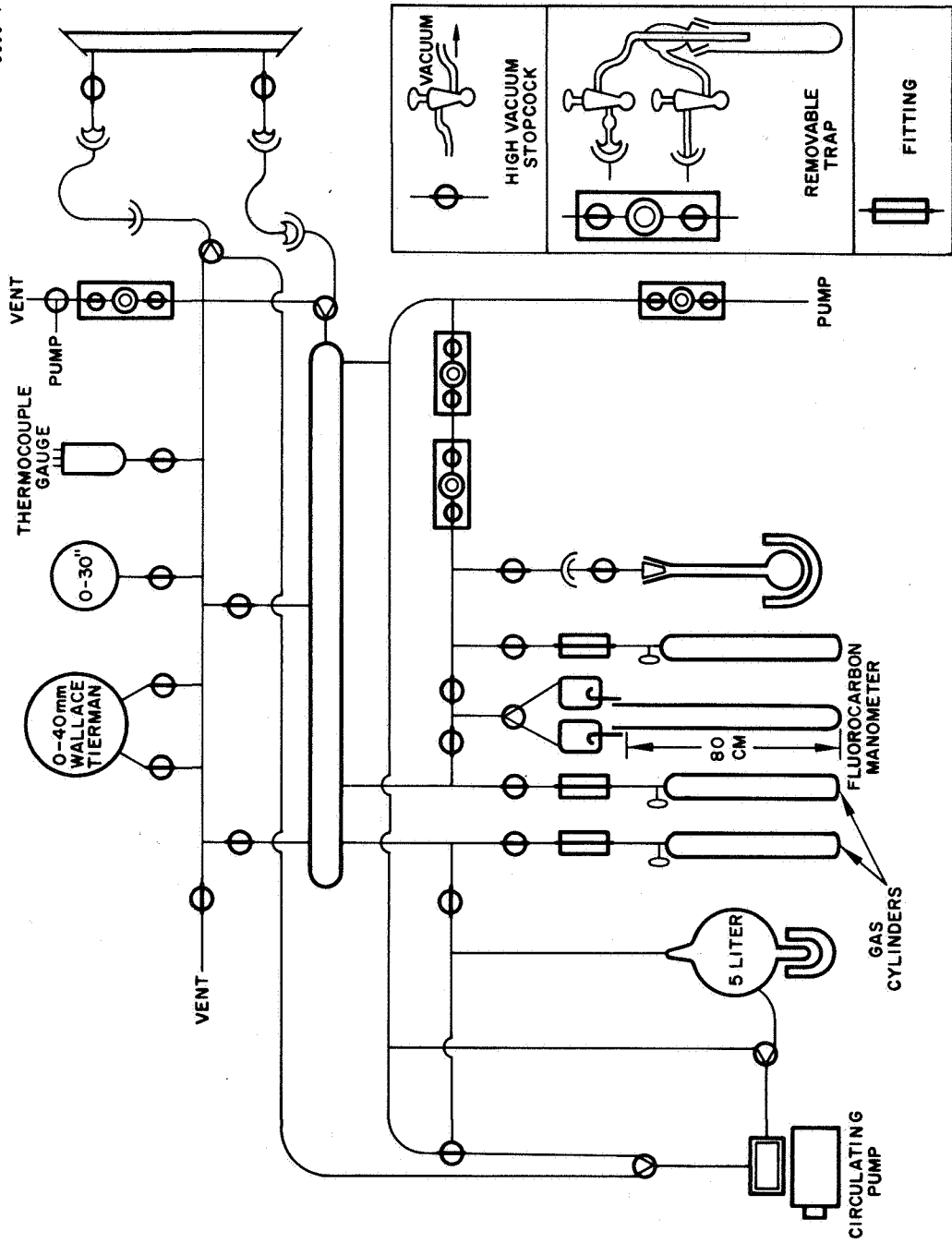


Fig. 54. Schematic of gas handling system.

TABLE X

Detectors Available for Photochemical Laser Studies

Type	Temp., °K	Window Material	Useful Range, λ , μ	Peak Detectivity, D^*_{λ} $\text{cm cps}^{1/2}/\text{W}$	Response Time, μsec
S-1 Photomultiplier (RCA-7102)	194	glass	0.5 to 1.2	1×10^{13}	<1
PbS (Ektron)	295	none	1 to 3.5	8×10^{10}	0.7×10^3
PbS	194	infrasil	1 to 4	1×10^{11}	3×10^3
InAs (PC)	295	sapphire	1 to 4	1.4×10^8	0.2
InSb, PEM (SBRC)	295	none	1 to 7.5	3×10^8	0.2
InSb, PC (Philco)	77	sapphire	1 to 5.9	3×10^{10}	2
Thermopile (Eppley)	295	KBr	0.4 to 25 μ		0.5×10^6
Thermopile (Reeder)	295	diamond	>1	1×10^9 max (50 to 200 μ)	30×10^3
Golay Cell (Eppley)	295	diamond	>1	1.7×10^9	20×10^3
Ge:Au	77		1 to 9	1.8×10^{10}	1
Ge:Ga	4	polyethylene and crystal quartz	40 - 110		1

experiments. Two mechanical vacuum pumps are utilized in the system. One is primarily for gas purification procedures, vacuum distillations, and evacuation of the gauge and manometer sections. The second pump is used for sample handling and evacuation of the laser tube. Several gauges are incorporated for pressure measurements in different ranges. These include a thermocouple gauge, a manometer filled with fluorocarbon fluid (3M, FC-43), and two metal bourdon gauges. The compounds to be studied are introduced from lecture bottles connected to the system with Monel tubing, or from glass reservoirs. Samples can be taken through several traps for purification and can be mixed with other gases in a 5 liter expansion bulb attached to the manifold. The mixed sample can then be transferred into or flowed through the laser tube.

TABLE XI
Broad-Band Infrared Filters

Wavelength Range, μ	Long λ Pass – Long λ Reject
1.8 to 3.5	Ge – Vicos
3.5 to 6.0 (5.5)	Te – TiO ₂
3.5 to 6.5	Te – LiF
7 to 14	InSb – BaF ₂
7 to 15	InSb – Irtran II
40+	Black polyethylene + crystal quartz
50+, 60+, 70+, 80+, 90+, 100+, 125+, 150+	Special polyethylene compound filters

C. PHOTOLYSIS OF CF₃I: IODINE ATOM LASER

Experimental results obtained from flash photolysis of trifluoromethyl iodide are shown in Figs. 55 to 63. A number of experiments were carried out with this compound, and the results reported here are representative of the variety of experimental conditions employed. Figures 55 and 56 show the temporal behavior of the laser power output at a series of pressures from 20 to 0.5 Torr CF₃I. The flash-lamp emission was monitored separately and is illustrated on the lower trace of Figs. 55 and 56. Both the laser power and energy available from the CF₃I system are seen to depend strongly on CF₃I pressure. As shown in Fig. 55(a), and 55(b), greater power is obtained at 20 Torr than at 10 Torr CF₃I, but laser emission is quenched sooner at the higher pressure. As the pressure is reduced to 2.5 Torr (Fig. 56(a)), laser emission becomes quasicontinuous, with considerably less spiking than at higher pressures. No emission could be observed from 0.5 Torr CF₃I with the apparatus used in these experiments. As discussed earlier, molecular iodine is an efficient quencher of excited iodine atoms; its formation and subsequent deactivation of I(²P_{1/2}) are thought to be responsible for cessation of laser action.

Variation of the flashlamp discharge voltage with constant capacitance (25 μF) in the circuit was used to study the effect of pumping intensity on the behavior of the CF₃I system. These results are shown in Fig. 57. A pressure of 10 Torr CF₃I was used throughout, and the flashlamp discharge voltage was varied from 8 to 4.5 kV; the lower limit was determined by the minimum value required to fire the lamp. Both the flash lamp and laser output are delayed relative to their value at 8 kV as the discharge voltage is decreased. Although the laser action begins at approximately the same time relative to the flash lamp, both laser power and energy output are significantly reduced as the pumping intensity is decreased by a factor of 3. Threshold could not be observed in this set of experiments because of the flash lamp limitation mentioned above, but 200 J (with a rise time of ~40 μsec) is a conservative estimate.

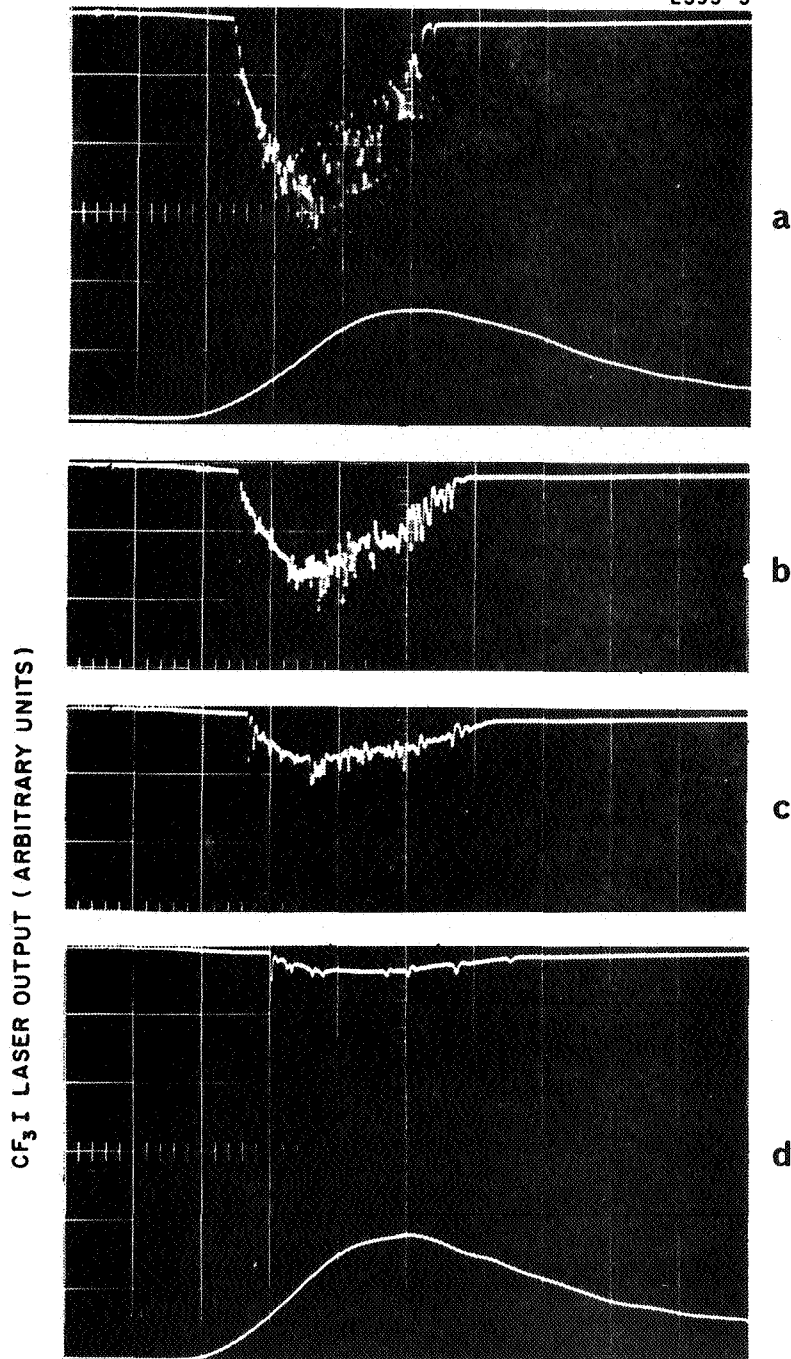


Fig. 55.
 CF_3I laser output (1.3μ), at different pressures. InAs(PC) detector. Time scale = $20 \mu\text{sec/div}$. Flashlamp output shown on lower trace monitored in ultraviolet-visible region. Excitation energy = 800 J ($25 \mu\text{F}$, 8 kV). (a) 20 Torr CF_3I ; no buffer gas; (b) 10 Torr CF_3I ; (d) 2.5 Torr CF_3I .

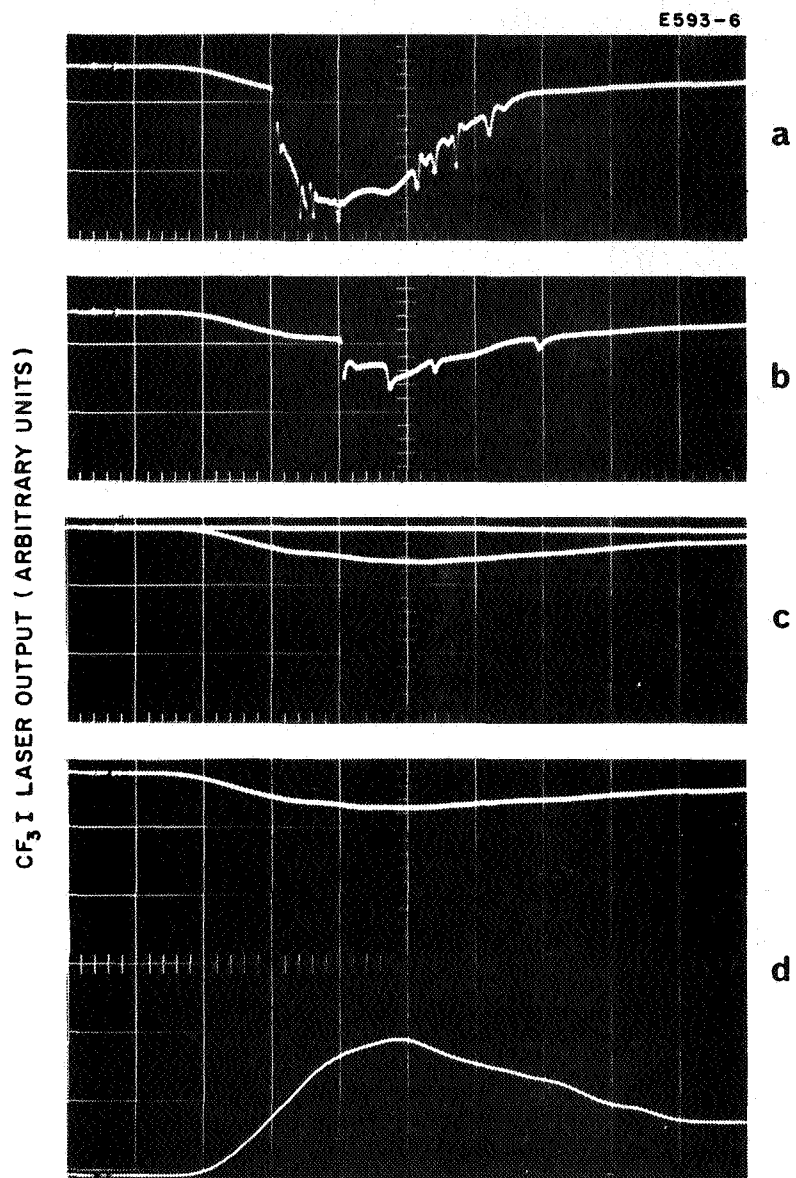


Fig. 56.
CF₃I laser output (1.3 μ) at lower pressures.
Time scale = 20 μ sec/div; InAs(PC) detector;
800 J excitation energy. (a) 2.5 Torr CF₃I;
(b) 1 Torr CF₃I; (c) 0.5 Torr CF₃I; (d) 0 Torr
CF₃I.

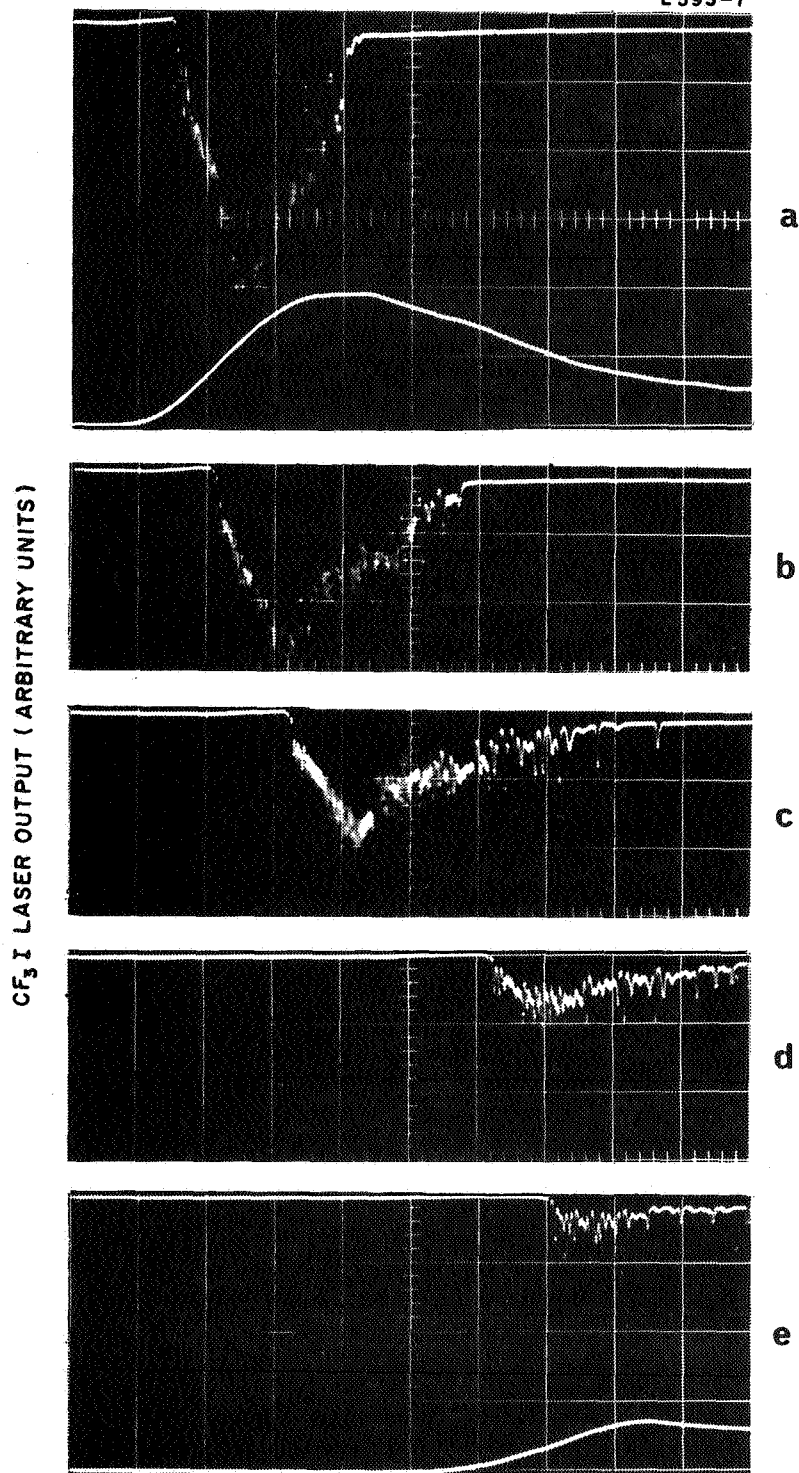


Fig. 57.
CF₃I laser output at
different flashlamp
discharge voltages.
C = 25 μ F, CF₃I pres-
sure = 10 Torr; InSb
(PEM) detector; time
scale = 20 μ sec/div.
(a) 8 kV; (b) 7 kV;
(c) 6 kV; (d) 5 kV;
(e) 4.5 kV.

The temporal behavior of the CF_3I system is shown on an expanded time scale in Fig. 58 with 20 Torr CF_3I and an excitation energy of 612 J (25 μF , 7 kV). Laser action occurs for 80 μsec under these conditions; the pumping source has a duration of 200 μsec with 100 μsec width at half height. Figure 59 illustrates the effect of excitation (pumping) energy on the laser output using constant discharge voltage (intensity). Note that the initial flash lamp intensity (rise time) is comparable in both Fig. 59(a) and 59(b) and that laser action terminates near the maximum of both pumping pulses; however, the laser power and energy output is considerably greater at the higher excitation energy. Further increase of pumping energy (1200 J) does not result in a substantial increase of the laser output at this particular pressure.

The performance of the CF_3I system was also studied under conditions of added optical cavity loss. Results from extreme conditions are shown in Fig. 60. The upper trace in Fig. 60(a) shows laser output at 5 Torr CF_3I with no loss introduced into the cavity. Figure 60(b) shows the signal from the laser detector at maximum sensitivity when one of the cavity mirrors was excluded from the optical system. This trace represents pickup from the flashlamp only, and does not show continuous laser output. (The flashlamp profile is not shown in Fig. 60(a), (c) or (d), however, because of different gain settings.) The traces in Fig. 60(c) and 60(d) show the laser output when the CF_3I pressure is raised to 10 Torr and one cavity mirror is excluded. Usually only one pulse occurred as in Fig. 60(c) after the pumping source had reached maximum intensity; sometimes, as shown in Fig. 60(d), a second smaller pulse was also produced. The detector attenuation used in Fig. 60(c) and 60(d) was similar to that in Fig. 60(a) so the intensity of the single pulses obtained in this way are comparable to those obtained in normal operation, i. e., the outputs displayed by the traces in Fig. 60(c) and (d) are not to be construed as giant pulses obtained by Q-switching. The trace shown in Fig. 60(e) indicates the absence of laser action when both cavity mirrors are excluded and the CF_3I pressure is raised to 37 Torr. The traces in Fig. 60(a) to 60(e) were obtained with constant flashlamp excitation energy and intensity (800 J, 25 μF , 8 kV).

CF₃I LASER OUTPUT (ARBITRARY UNITS)

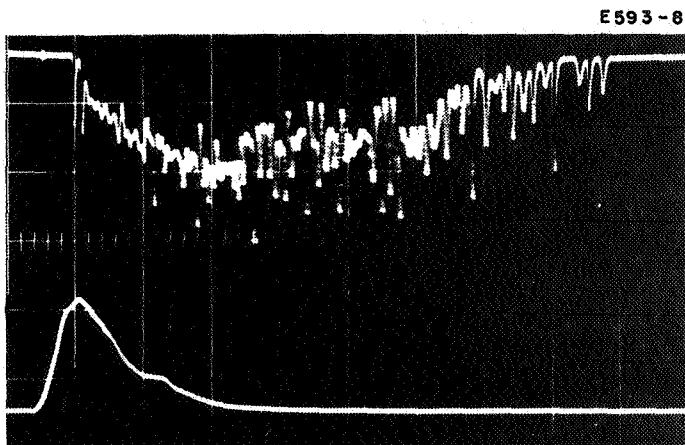
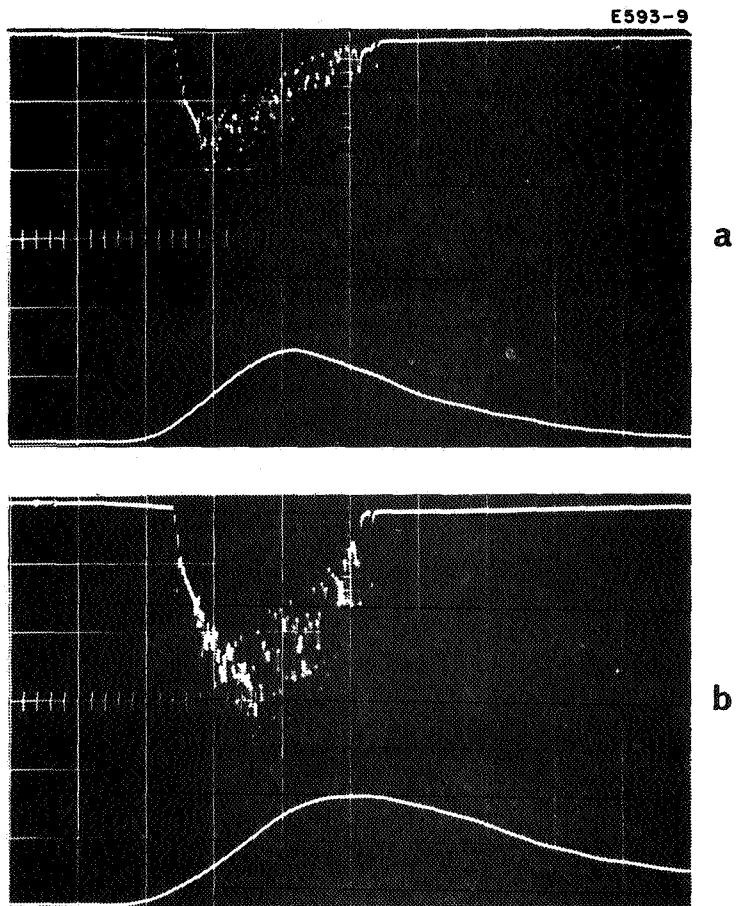
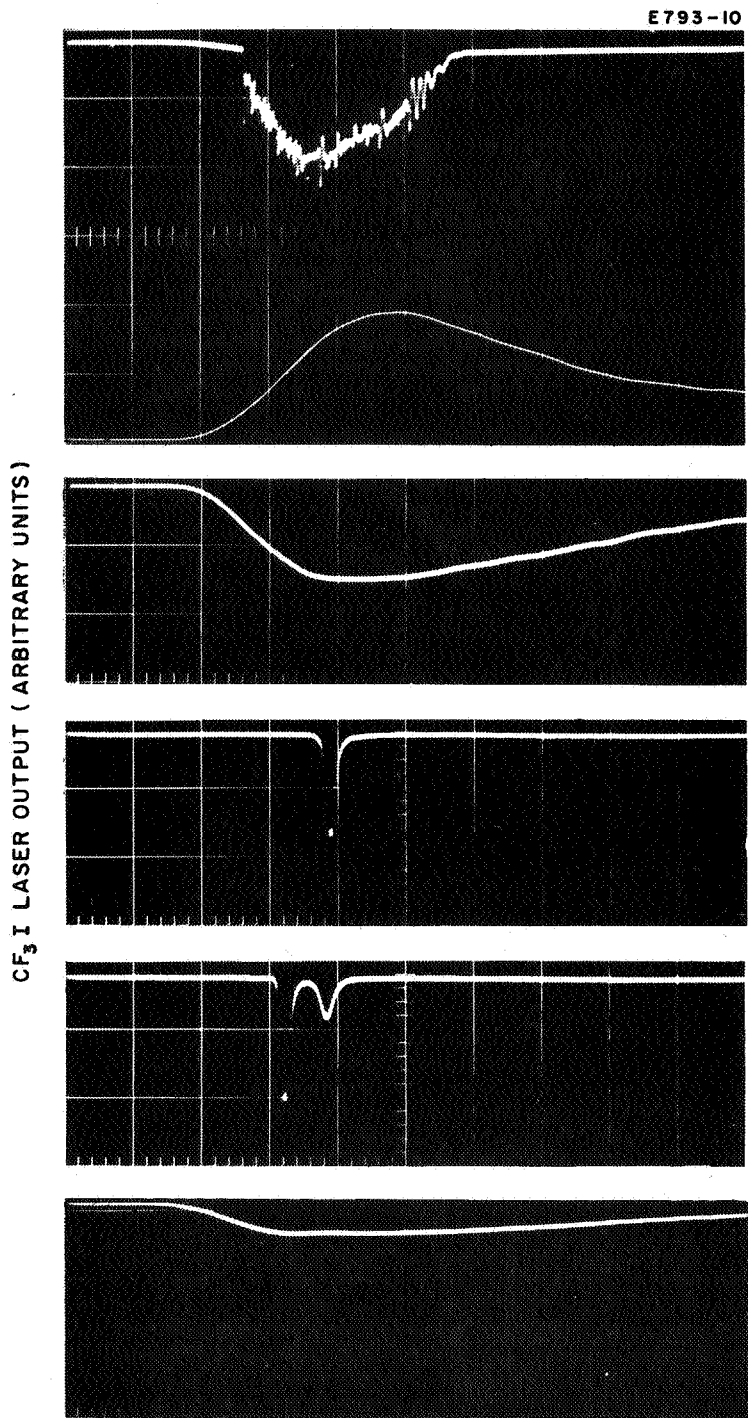


Fig. 58.
CF₃I laser output (upper trace); CF₃I pressure = 20 Torr; flashlamp energy = 612 J (25 μ F, 7 kV); InAs (PC) detector; time scale: lower trace = 100 μ sec/div upper trace = 10 μ sec/div.

Fig. 59.
CF₃I laser output at different excitation energies. CF₃I pressure = 20 Torr; InAs (PC) laser detector, time scale = 20 μ sec/div; lower trace, flashlamp monitor. (a) 12.5 μ F, 8 kV (400 J); (b) 25 μ F, 8 kV (800 J).

CF₃I LASER OUTPUT (ARBITRARY UNITS)





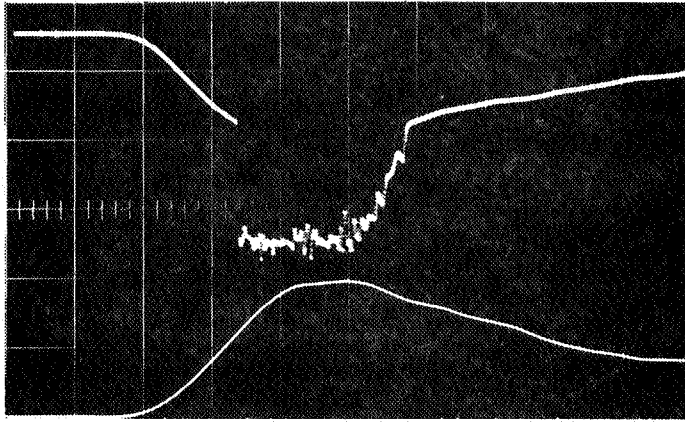
a
b
c
d
e

Fig. 60.
CF₃I laser output
with extreme cavity
loss. Excitation
energy = 800 J (25 μF,
8 kV). (a) No added
loss, CF₃I pressure =
5 Torr, 20 μsec/div;
(b) one cavity mirror
excluded, 5 Torr CF₃I,
20 μsec/div, trace
shows flashlamp out-
put only (detector
sensitivity 10x other
traces; (c) and (d)
one cavity mirror
excluded, 10 Torr
CF₃I, 20 μsec/div.

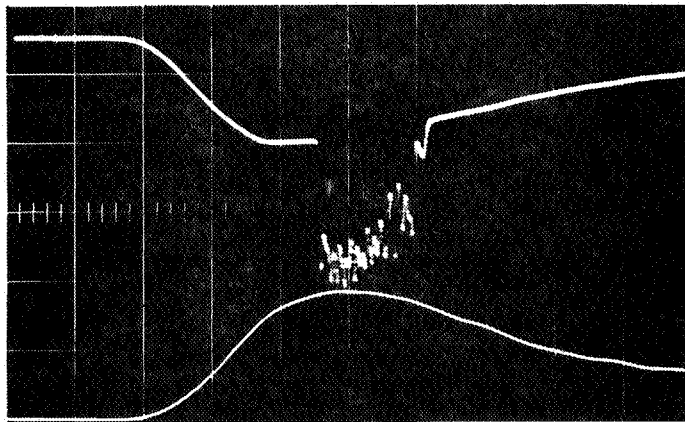
Laser output obtained from 5 Torr CF_3I with 800 J pumping energy, when calibrated optical loss was inserted in the cavity, is illustrated in Fig. 61. In these traces the flashlamp profile is superimposed on the laser detector because minimum optical filtering and attenuation was needed. The onset of laser action is delayed in these experiments as the cavity insertion loss is increased from 4 to 19 dB. (Optical loss in decibels equals 10 times optical density.) Results of experiments at a higher pressure of CF_3I (7.5 Torr) and at different pumping intensities are shown in Figs. 62 and 63.

The observation of significant delays in the laser output in the experiments with large cavity losses suggested the possibility of an over-all delay in laser quenching by molecular iodine. Because of an increase in the lifetime of atomic iodine in the absence of stimulated emission, iodine formation could be delayed if excited iodine atoms do not recombine. The results for 5 Torr CF_3I are shown in Fig. 64. This possibility was investigated further under conditions for which the delay was expected to be maximized — 1200 J excitation energy (37.5 μF , 8 kV), 7.5 Torr CF_3I , and 25 dB loss in the cavity. However, this series of experiments showed the increase in delay time for laser action in the high loss situation over the termination of laser action in the low loss case to be less than 5 μsec ; it was not reproducible to less than this amount. Hence the earlier indications were not substantiated, although an exhaustive study was not made.

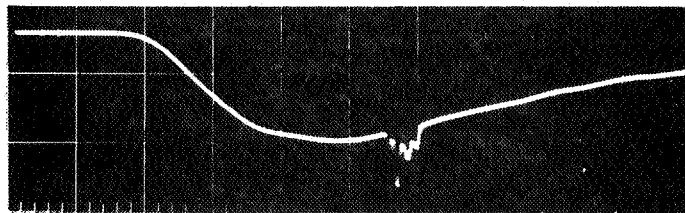
The variation of laser onset, duration, and termination as a function of cavity loss with 5 Torr CF_3I is summarized in Fig. 64. The time delay (measured from the flashlamp onset) before laser initiation and termination both increase linearly with optical loss in the cavity. The time period over which laser action occurs under these conditions is given by the difference between the two curves at a particular value of cavity loss.

CF₃I LASER OUTPUT (ARBITRARY UNITS)

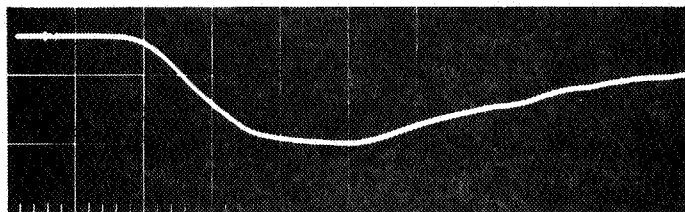
a



b

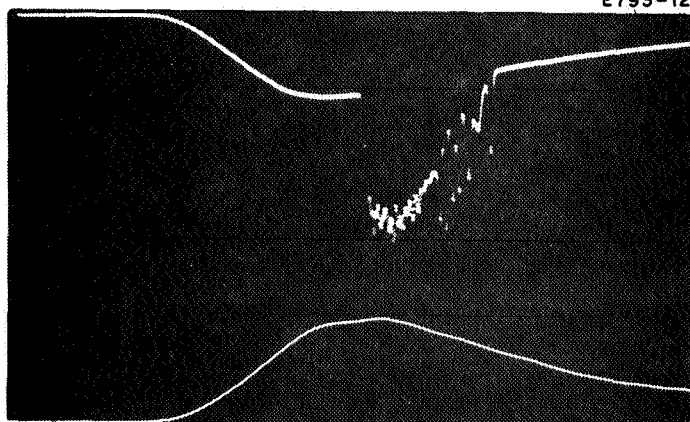


c

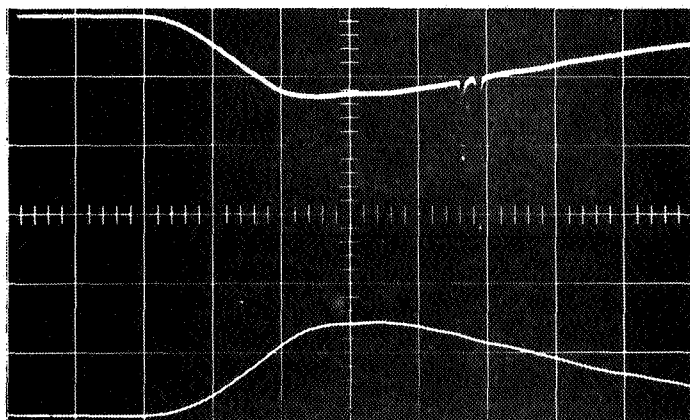


d

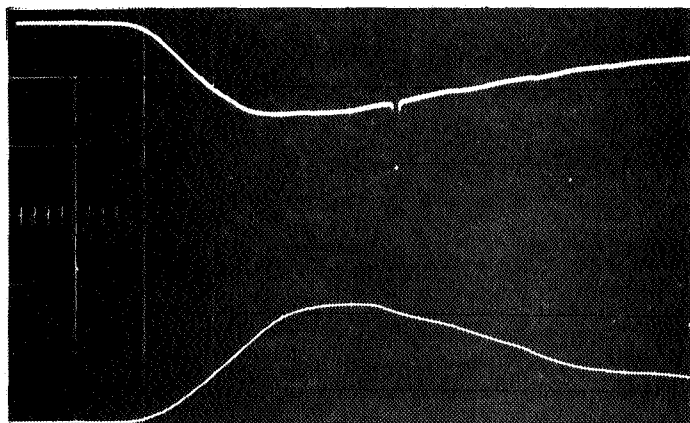
Fig. 61.
 CF₃I laser output
 with calibrated optical
 loss introduced in
 cavity. CF₃I pres-
 sure = 5 Torr; excita-
 tion energy = 800 J
 (25 μ F, 8 kV),
 20 μ sec/div, active
 length of laser tube =
 1 m. (a) 4.2 dB;
 (b) 12 dB; (c) 17.5 dB;
 (d) 19 dB.

CF₃I LASER OUTPUT (ARBITRARY UNITS)

a



b

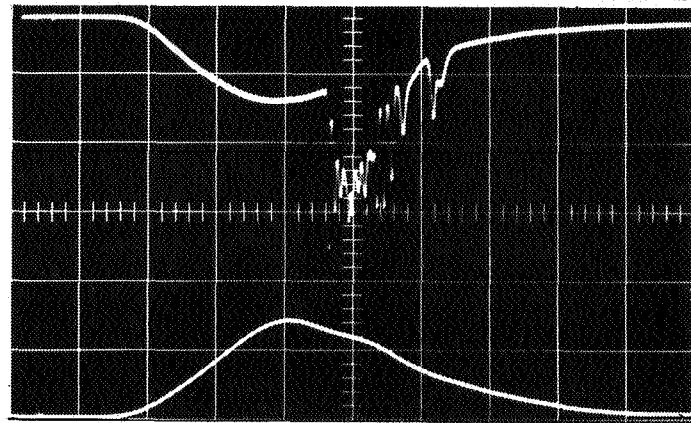


c

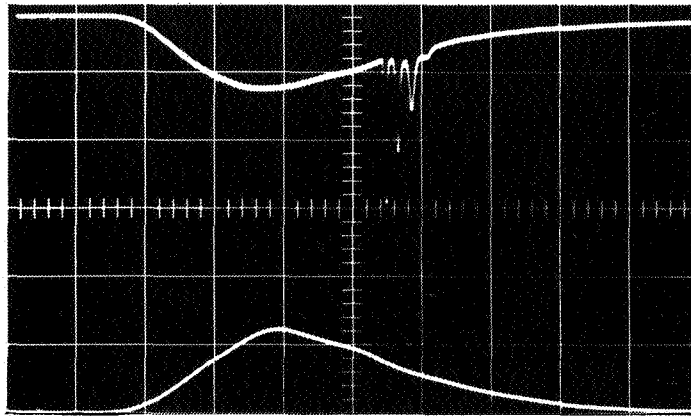
Fig. 62.

CF₃I laser output with calibrated optical loss in cavity at different excitation intensities.

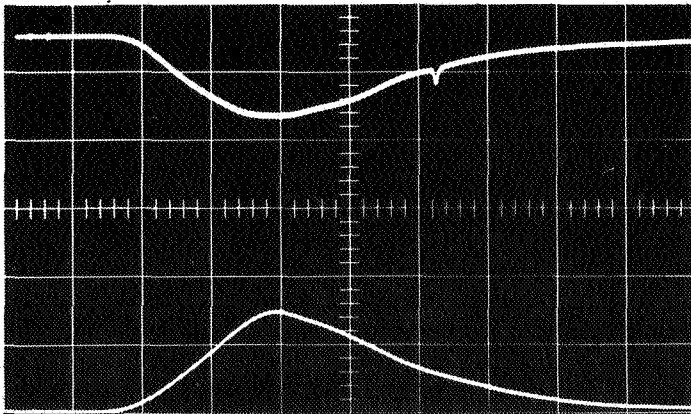
Time scale = 20 μsec/div, CF₃I pressure = 7.5 Torr (a) 15 dB, 612 J (25 μF, 7 kV); (b) 23 dB, 612 J (25 μF, 7 kV); (c) 26 dB, 800 J (25 μF, 8 kV).

CF₃I LASER OUTPUT (ARBITRARY UNITS)

a



b



c

Fig. 63.
 CF₃I laser output with calibrated optical loss in cavity. CF₃I pressure = 7.5 Torr, excitation energy = 400 J (12.5 μF, 8 kV), time scale = 20 μsec/div.
 (a) 15 dB; (b) 19 dB;
 (c) 21 dB.

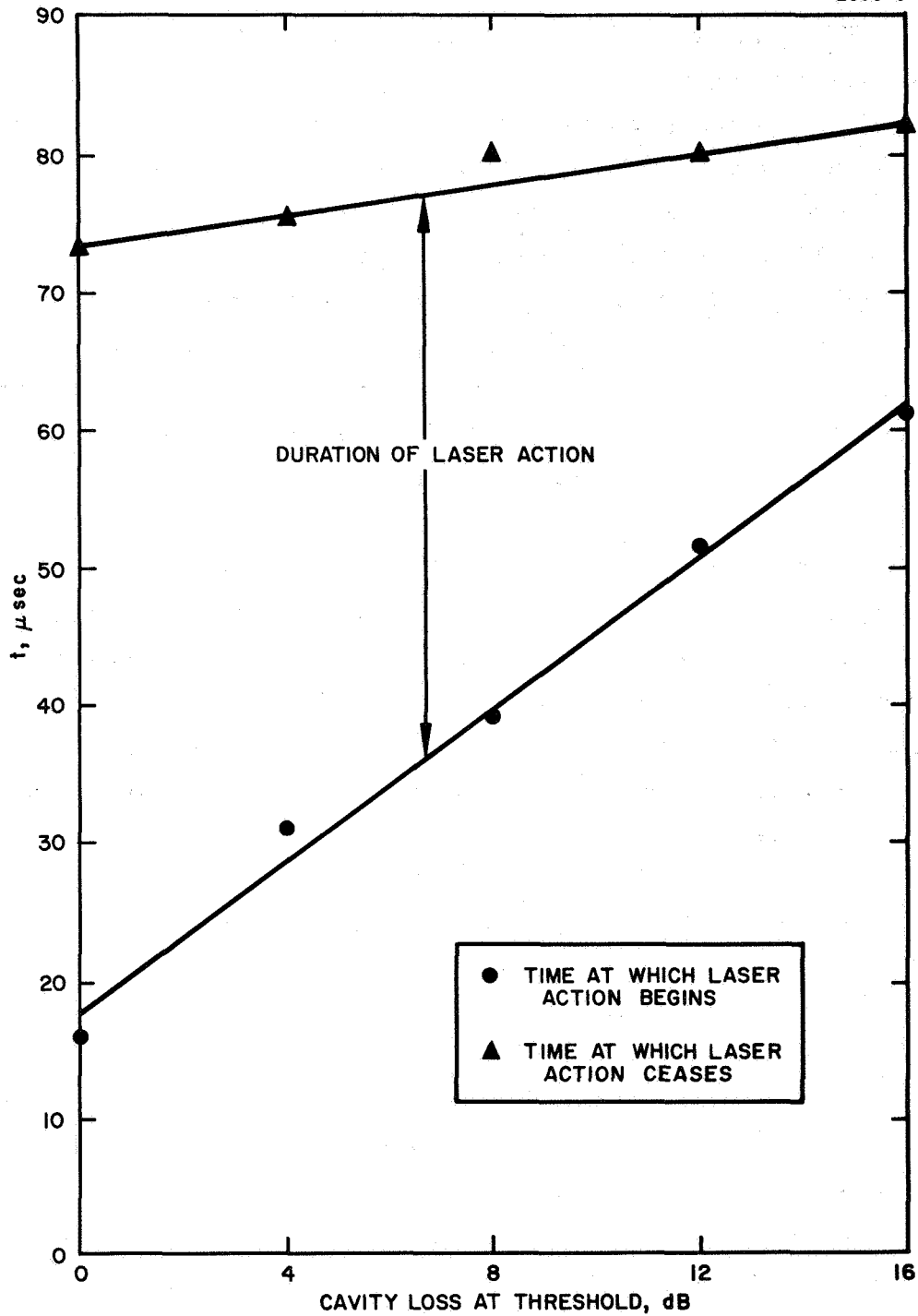


Fig. 64. Variation of onset, termination, and duration of laser oscillation from CF_3I versus cavity loss. CF_3I pressure = 5 Torr, excitation energy = 800 J (25 μF , 8 kV).

The gain of the CF_3I photodissociative laser can be inferred from experiments of the type discussed above. With the CF_3I pressure and the pumping parameters kept constant, calibrated losses are inserted in the cavity until laser action is barely perceptible. This loss plus the residual cavity losses (estimated as 1 dB) represent the gain of the active material under the particular conditions employed. Measurements of this quantity were made at a series of pressures over the range 1 to 7.5 Torr and at different pumping intensities. These experiments are summarized in graphical form in Figs. 65 and 66. The gain of the CF_3I system plotted versus CF_3I pressure shows significant deviation from linearity at 7 Torr. Other workers have reported a value of 106 dB/m at 90 Torr CF_3I , which is considerably less than that estimated from extrapolation of the low pressure (5 Torr) results. These results are consistent with and add further support to laser termination in this system by a quenching agent photochemically formed in higher yields at higher pressures. As expected, the gain of the system at constant pressure increases linearly with excitation intensity at low intensities and begins to saturate at high intensities, as shown in Fig. 66.

D. PHOTOLYSIS OF NOCl :NITRIC OXIDE LASER

Emission (5.95 to 6.3 μ) from the nitrosyl chloride photodissociative laser system is illustrated in Fig. 67. The temporal characteristics are considerably different from the CF_3I system. Fewer pulses are observed in the NOCl -He system and operation is mainly on a quasicontinuous basis as shown in the figure. Trace (c) in Fig. 67 is not caused by scattered light from the flashlamp, which is monitored on the lower trace using the same time scale on both traces. Thus laser action occurs early in the pumping pulse and is quenched before the flashlamp reaches its maximum intensity. Only ~5% of the pump energy used in these experiments is expended before

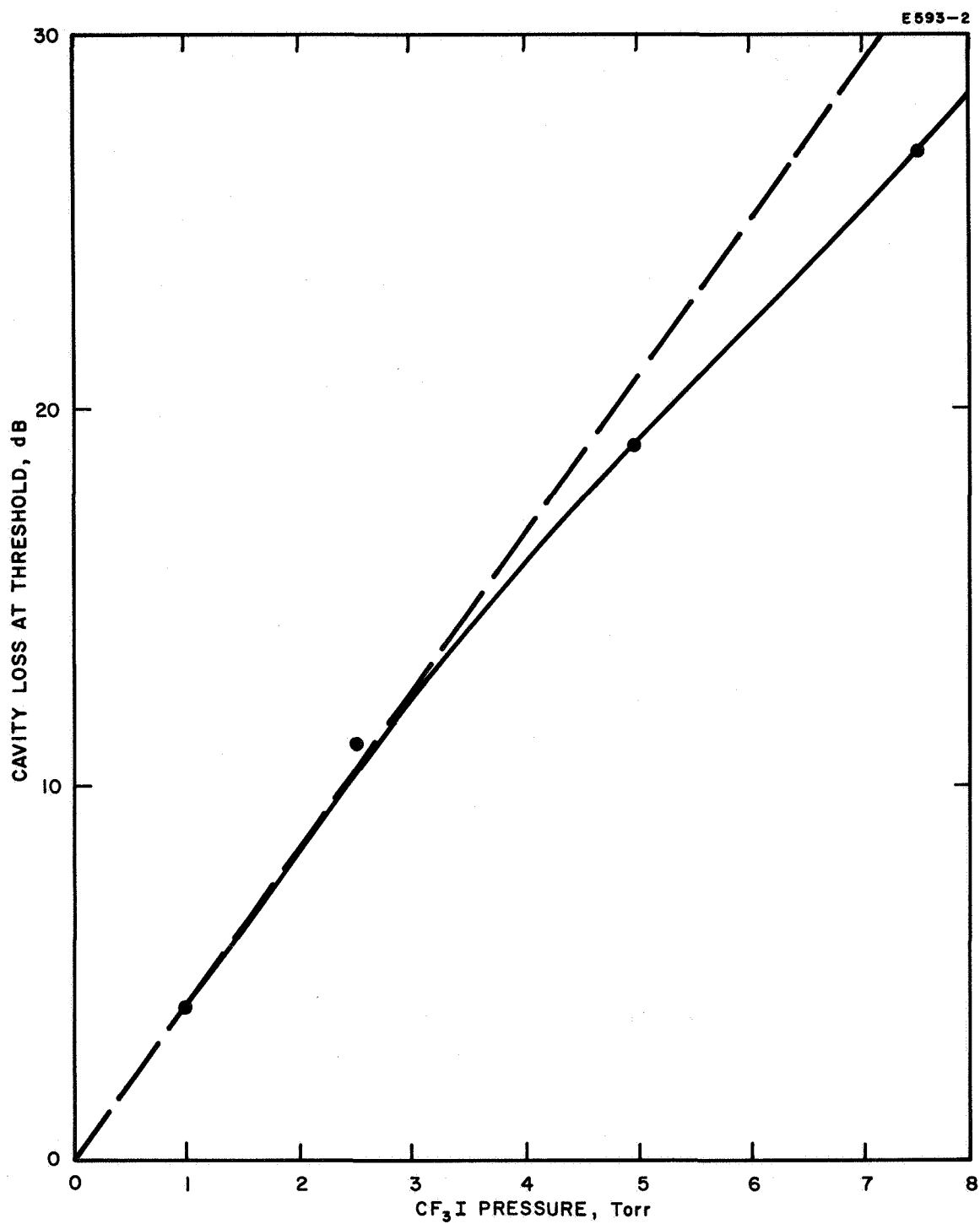


Fig. 65. CF₃I gain in lower pressure region. Excitation energy = 800 J (25 μ F, 8 kV), laser tube dimensions: length = 1 m, diameter = 10 mm.

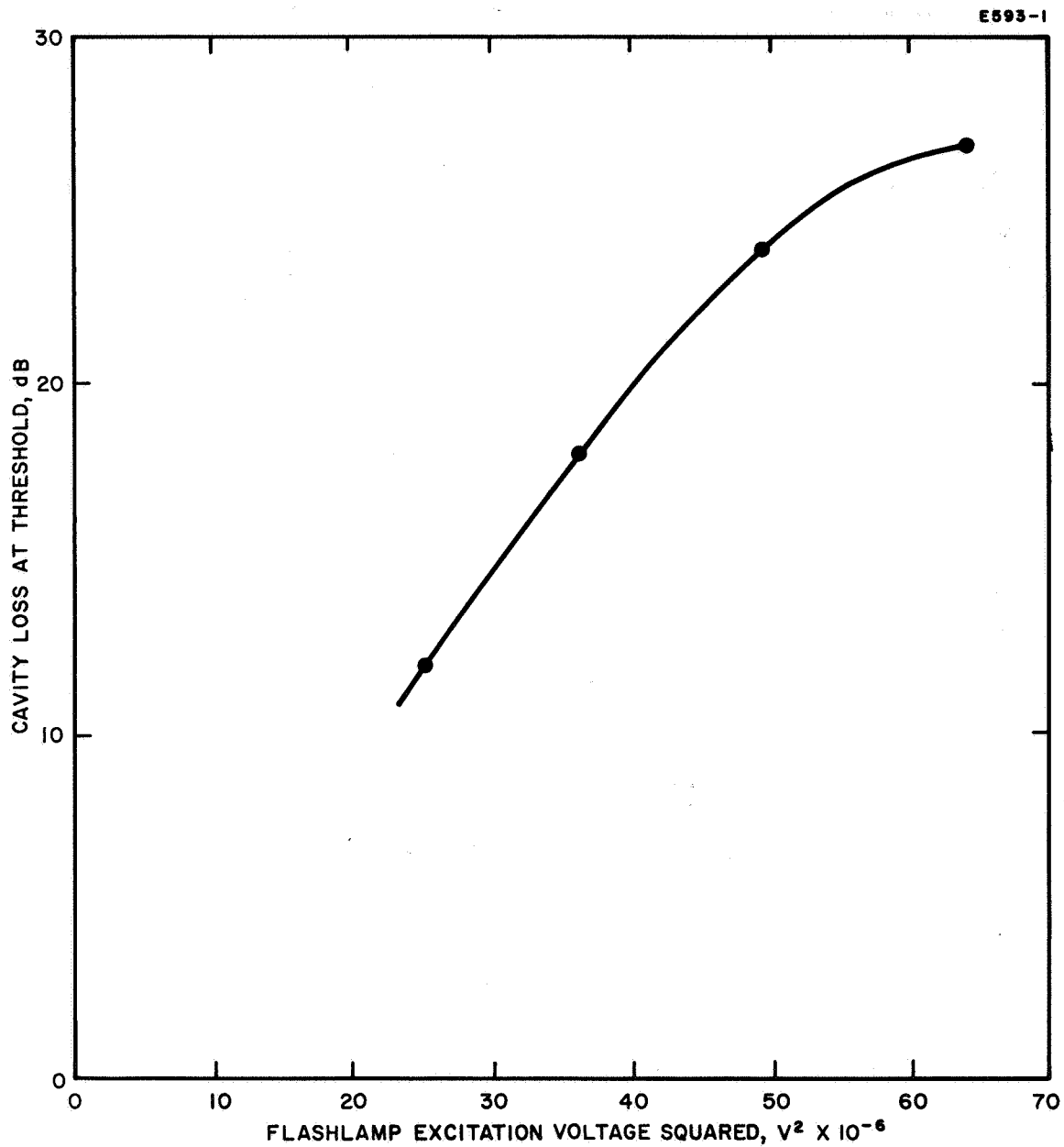


Fig. 66. CF_3I laser gain versus flashlamp intensity. CF_3I pressure = 7.5 Torr, flashlamp capacitor = 25 μF , laser tube dimensions: length = 1 m, diameter = 10 mm.

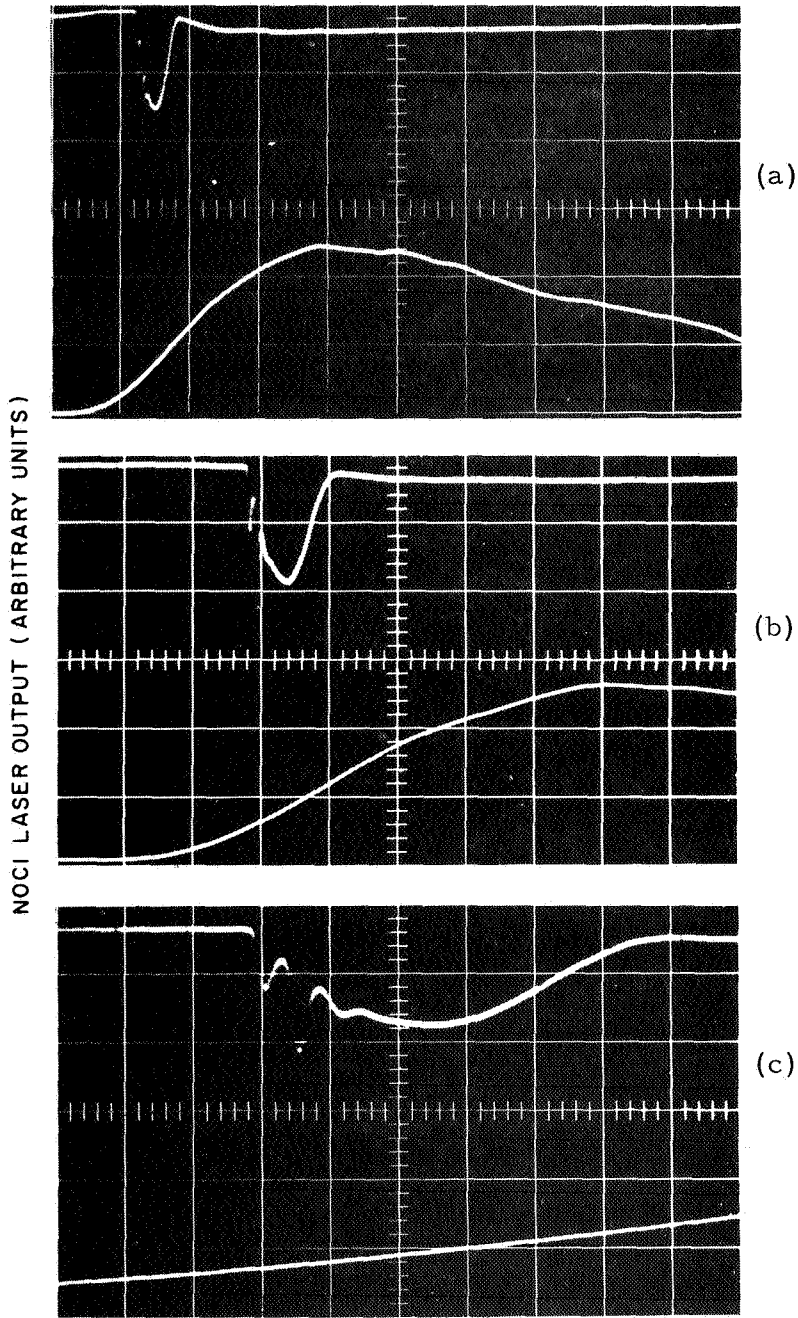


Fig. 67.
Output from nitrosyl chloride photodissociative laser. Helium used as buffer gas; total pressure = 90 Torr (~ 4 Torr NOCl). InSb (PEM) detector; lower trace shows flashlamp profile on same time scale as laser monitor (upper trace); excitation energy = 1200 J ($37.5 \mu\text{F}$, 8 kV). Time scale = (a) $20 \mu\text{sec/div}$; (b) $10 \mu\text{sec/div}$; (c) $2 \mu\text{sec/div}$.

laser action is terminated. The quenching mechanism has not yet been deduced, although further studies in this direction are in progress. The effects of excitation energy and intensity on the laser output are shown in Figs. 68 and 69. Under the conditions employed, threshold is reached when 300 J are discharged through the flash lamp with a rise time of 30 μ sec. The actual energy threshold is considerably less since only a small fraction is utilized before laser action is terminated. Figure 70 shows the laser output from this system at a series of NOCl and helium pressures with constant pumping energy (1200 J, 37.5 μ F, 8 kV).

One of the anticipated advantages of this system is the known chemical conversion of photolysis products (Cl_2 and NO) to NOCl. The elementary reaction in this process is third-order, and hence the time required for conversion is quite large when the initial pressure of NOCl is low. A series of experiments have been carried out with various mixtures of helium and nitrosyl chloride, helium-chlorine-nitrosyl chloride, and chlorine-nitrosyl chloride mixtures to determine the maximum pressure of nitrosyl chloride and optimum amounts of added gases which could enhance chemical reversibility and laser performance of this system.

The maximum partial pressure of nitrosyl chloride in NOCl-He mixtures from which laser action could be observed is 6.25 Torr, with total pressures from 50 to 125 Torr. Laser action could not be detected from NOCl-He mixtures with NOCl partial pressures from 6.5 to 10 Torr and total pressures ranging from 65 to 300 Torr using maximum detection sensitivity and excitation intensity. Optimum pressure for the NOCl-He system with regard to laser energy and power output appears to be in the range 3 to 5 Torr NOCl and 40 to 150 Torr helium, with the partial pressure of helium far less critical than the amount of nitrosyl chloride. The time for conversion of NO and Cl_2 formed in the photolysis of mixtures of this type is too great to be of practical value in most applications. The chemical process is

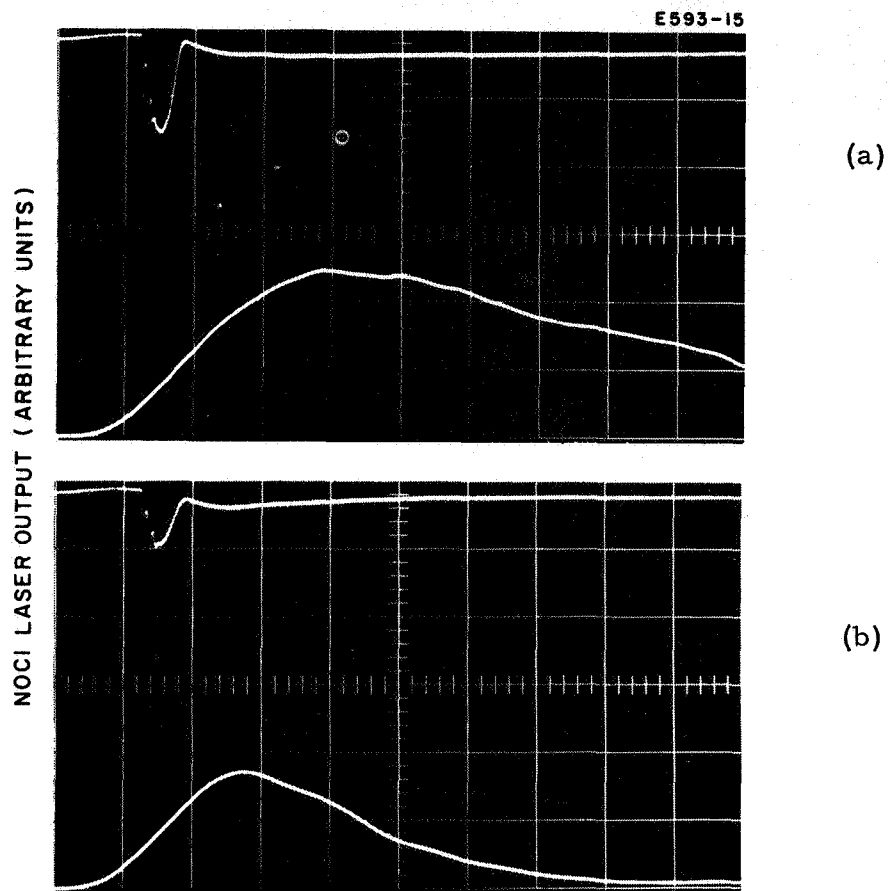


Fig. 68.
Effect of excitation energy on NOCl laser output. Buffer gas, helium; total pressure = 90 Torr (~ 4 Torr NOCl); time scale = 20 $\mu\text{sec}/\text{div}$. (a) 1200 J (37.5 μF , 8 kV); (b) 400 J (12.5 μF , 8 kV).

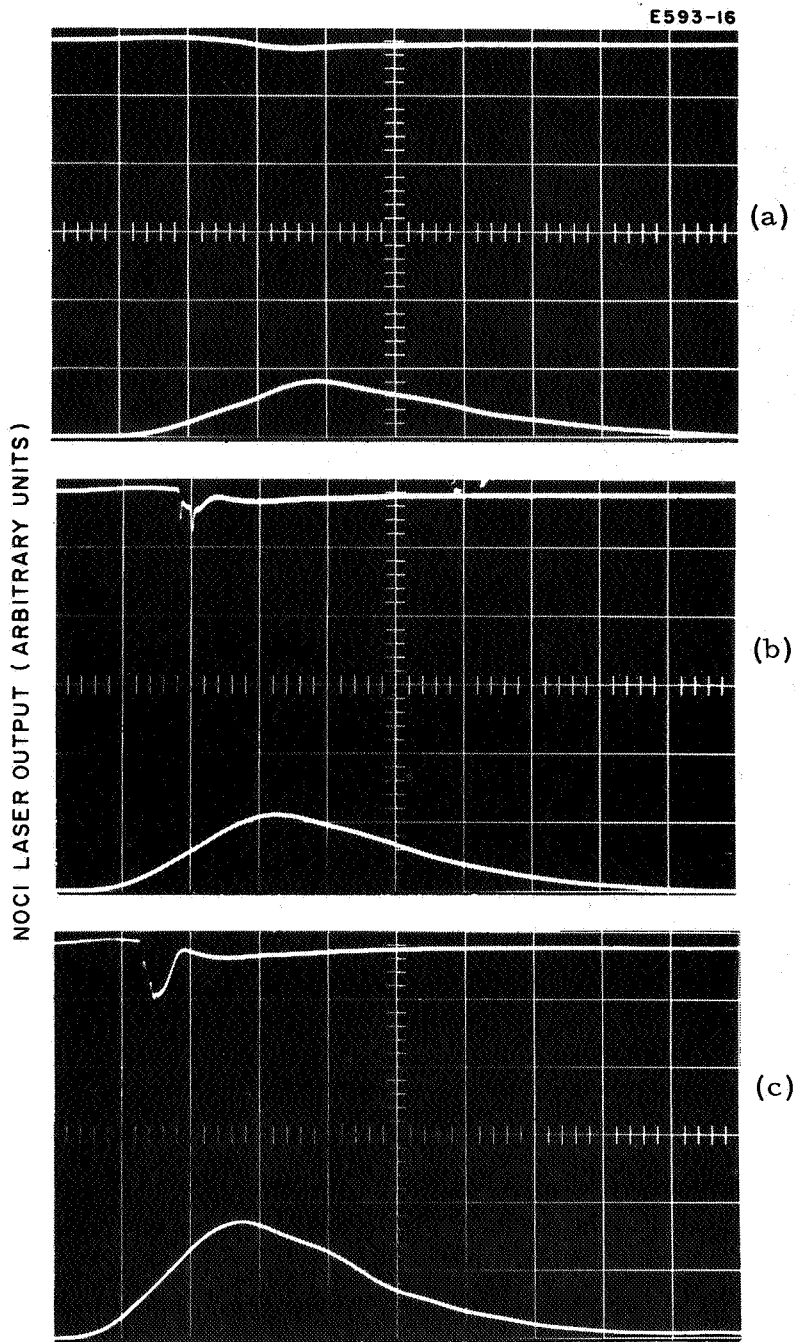


Fig. 69.
 Effect of excitation intensity on NOCl laser output. Buffer gas, helium; total pressure = 90 Torr (~ 4 Torr NOCl). Time scale = 20 μ sec/div; flashlamp intensity varied by discharging different voltages through a 12.5 μ F capacitor. (a) 6 kV (225 J), below threshold; (b) 7 kV (306 J); (c) 8 kV (400 J).

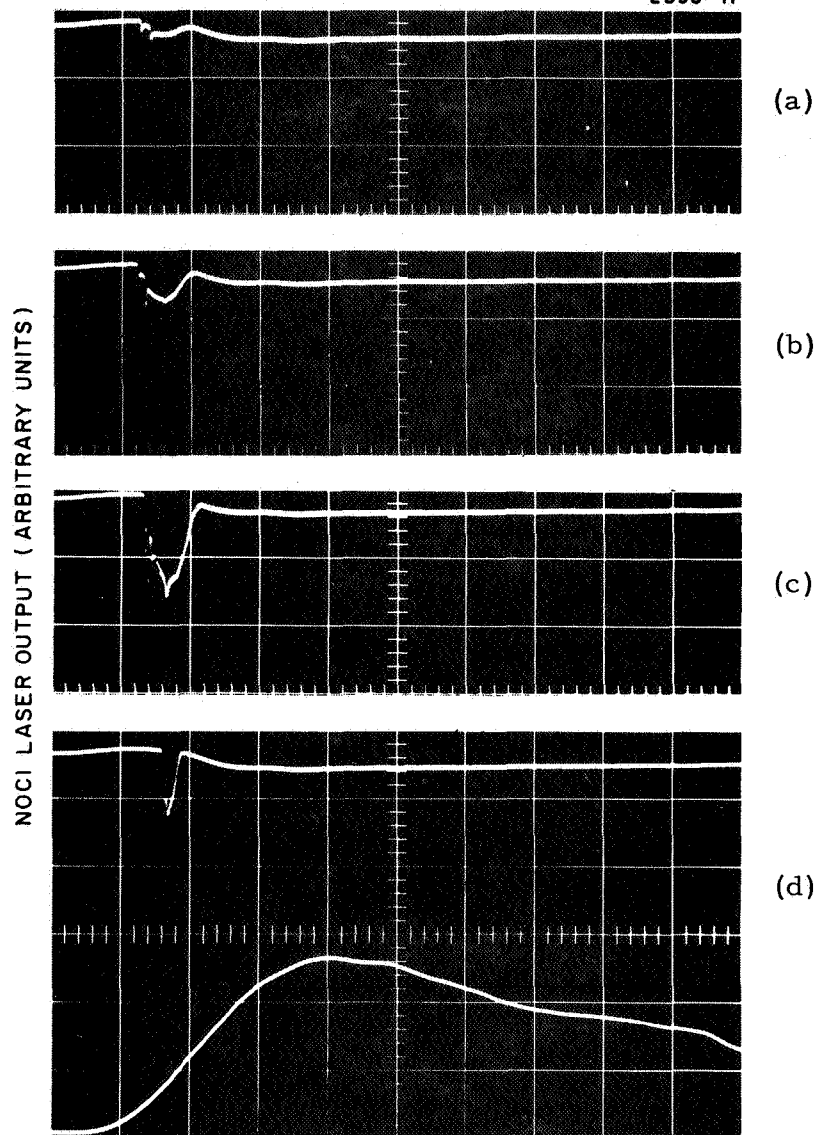
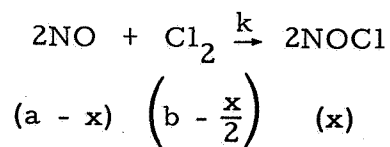


Fig. 70.
 Laser output from nitrosyl chloride. Helium mixture ($P_{\text{NOCl}}/P_{\text{total}} = 1/40$). Excitation energy = 1200 J (37.5 μF , 8 kV); time scale = 20 $\mu\text{sec}/\text{div}$. (a) total pressure = 20 Torr, NOCl pressure = 0.5 Torr; (b) total pressure = 40 Torr, NOCl pressure = 1 Torr; (c) total pressure = 100 Torr, NOCl pressure = 2.5 Torr; (d) total pressure = 200 Torr, NOCl pressure = 5 Torr.



and the rate of reaction is given by

$$\frac{dx}{dt} = k(a - x)^2 \left(b - \frac{x}{2} \right),$$

which when integrated by the method of partial fractions gives

$$\frac{2}{(2b - a)^2} \left[\frac{(2b - a)x}{a(a - x)} + \ln \frac{b(a - x)}{a \left(b - \frac{x}{2} \right)} \right] = kt.$$

a and b are the initial concentration of nitric oxide and chlorine, respectively; x is the concentration of nitrosyl chloride at time t ; and k is the rate constant for the process. When only nitrosyl chloride and helium are present initially, the integrated rate expression takes a simpler form, since after photolysis nitric oxide and chlorine will be in the ratio of 2:1, i.e., $a = 2b$. Making this substitution in the differential equation yields

$$\frac{dx}{dt} = \frac{k}{2} (a - x)^3,$$

which readily integrates to

$$\frac{1}{(a - x)^2} - \frac{1}{a^2} = \frac{k}{2} t.$$

The time $\tau_{1/2}$ required for 50% conversion of the nitric oxide and chlorine back to nitrosyl chloride is obtained from this relation; the known value of the rate coefficient is $k = 1.6 \times 10^7 \text{ cm}^6 \text{-mole}^{-2} \text{-sec}^{-1}$.

$$\tau_{1/2} = \frac{1.2 \times 10^8}{P_{(\text{mm})}^2} \text{ sec}.$$

Here P is the partial pressure of nitric oxide or initial pressure of nitrosyl chloride if photolysis results in 100% decomposition of NOCl. Thus it is clear that although the NOCl system is reversible in theory, the time required is far too great to be of practical value in most applications ($\tau_{1/2} = 14$ days for $P_{\text{NOCl}} = 10$ Torr).

Although preliminary studies have indicated that 5 Torr is an upper limit to the NOCl partial pressure which can be used in NOCl-He mixtures, other buffer gases may yield more favorable results with regard to reversibility of the system. Added gases are definitely required since laser action could not be observed from pure nitrosyl chloride in the pressure range from 1 to 100 Torr.

As is apparent from the rate equations above, addition of chlorine or nitric oxide would reduce the time required for conversion of photolysis products to nitrosyl chloride. For example, the half life $\tau_{1/2}$ for a 10:1 mixture of Cl_2 to NO is

$$\tau_{1/2} = \frac{2 \times 10^6}{P_{\text{NOCl}}^2} \text{ sec .}$$

Thus $\tau = 22$ hours for a helium-chlorine-nitrosyl chloride mixture with Cl_2 to NOCl in the ratio of 10:1 and a pressure of 5 Torr NOCl. A few experiments with mixtures of these three gases have been carried out recently in our laboratory. Preliminary results indicate that the maximum partial pressure of NOCl from which laser action can be observed is 4 Torr, although an exhaustive study was not undertaken. Laser action was also observed from several mixtures of Cl_2 and NOCl without a buffer gas. Reversibility of the nitrosyl chloride laser system was observed using a 1:20 mixture of NOCl to Cl_2 at a total pressure of 125 Torr. With this particular composition laser action was observed from the second photolysis of a mixture retained in the laser tube overnight ($\tau_{1/2} = 8$ hour). These experiments indicate that suitable mixtures of nitrosyl chloride and other gases can probably be found for

which laser energy and power output as well as chemical reversibility of the system are optimized with respect to each other. No experiments were carried out utilizing nitric oxide-nitrosyl chloride mixtures in this study, but this compound could also enhance the reversibility of the system. Since laser action is obtained from upper vibrational levels of NO, added NO would not be expected to quench the emission by population of the terminal laser level. Another technique which could be employed to enhance reversibility of the nitrosyl chloride laser when large excesses of permanent gases are not required is transfer of the mixture by condensation after photolysis to a smaller volume. The rate of the back reaction could be considerably increased because of the pressure increase in the small volume. Therefore, in this way the system could be isolated and have a duty cycle of a few minutes.

E. PHOTOLYSIS OF OTHER COMPOUNDS

Several other compounds of interest in this project were studied briefly. However, laser action was not observed from these compounds under the conditions employed — 1 to 40 Torr and maximum pumping intensity from the flashlamp and power supply [minimum rise time ($\sim 30 \mu\text{sec}$) and width at half-height of the lamp temporal profile ($\sim 100 \mu\text{sec}$)]. The compounds studied for which laser action was not observed in the 1 to 7 μ region are CF_3Br , IBr , BrCN , and NO_2 . Further studies with these and other compounds are in progress.